Acta Cryst. (1975). B31, 2007

The Crystal Structure of Sodium 7,7,8,8-Tetracyanoquinodimethanide at 80° C

BY M. KONNO AND Y. SAITO

The Institute for Solid State Physics, The University of Tokyo, Roppongi-7, Minato-ku, Tokyo 106, *Japan*

(*Received* 16 *January* 1975; *accepted* 17 *February* 1975)

The crystal structure of the high-temperature modification of Na^+TCNQ^- has been determined by X-ray diffraction at 80°C. The crystals are monoclinic with space group $P2_1/n$ and lattice constants: $a=3{\cdot}512$ (1), $b=11{\cdot}866$ (2), $c=12{\cdot}465$ (3) Å, $\beta=98{\cdot}21$ (2)° and $Z=2$. Weak reflexions with h and k both odd in the low-temperature phase disappeared completely at about 73°C. The intensity variations of two selected reflexions with temperature indicated that the transition is essentially first-order and the low- and high-temperature phases coexist in the range 59 to 73°C. The structure was refined by the full-matrix least-squares method to an R of 0·033 for the 675 observed reflexions collected by diffractometry. $TCNQ^-$ ions are stacked face-to-face to form columns along the a axis with an equal interplanar spacing of 3·385 Å above the transition temperature, whereas in the low-temperature phase they are arranged with alternate spacings of 3·21 and 3·49 Å and TCNQ dimers are present.

Introduction

In a previous paper (Konno & Saito, 1974) the crystal structure of the low-temperature modification of Na^+TCNQ^- was reported. The crystal structure of the high-temperature phase was determined by single-crystal X-ray diffraction, in order to gain a better understanding of the mechanism of the transition which occurs at 348 K (Vegter, Kuindersma & Kommandeur, 1971). In the present paper the crystal structure of Na^+TCNQ^- at 80°C is described.

Experimental

Crystals of Na^+TCNQ^- were kindly provided by Dr Sakai of this Institute. Preliminary zero-level Weissenberg photographs were taken with the crystal rotating around the c axis in the temperature range 25 to 85°C. The crystal was heated in a stream of electrically heated air. Weak 'uneven reflexions' with h and k both odd of the low-temperature phase were found to disappear at about 73°C. Moreover, it was observed that a twinned crystal (type (*a*) in the previous paper) transformed into a single crystal above 73°C. The crystal did not break down on passing through the transition temperature and the change was completely reversible. A crystal of dimensions $0{\cdot}38\times0{\cdot}25\times0{\cdot}13$ mm was mounted with the c axis parallel to the φ axis of the goniostat of a Rigaku manual diffractometer equipped with a heating device. The temperature of the crystal was kept constant at 80 ± 2°C during intensity collection. Reflexions with 2θ less than 40° were measured with Mo $K\alpha$ radiation monochromated by a graphite plate; the ω-scan technique was employed. Significant counts were recorded for 675 reflexions. Three standard reflexions were measured every three hours. The intensity data were corrected for Lorentz and polarization effects but no absorption correction was applied. In Table 1 the crystal data of the two modifications are compared.

Table 1. *Crystallographic data of low and high-temperature phases of* Na^+TCNQ^-

	$Na(C_{12}H_4N_4)$, F.W. 227·2	
	Low-temperature modification (23°C) Triclinic	High-temperature modification (80°C) Monoclinic
Space group	$C\bar{1}$	$P2_1/n$
a	6·993 (1) Å	3·512 (1) Å
b	23·707 (2)	11·866 (2)
c	12·469 (2)	12·465 (3)
α	90·14 (2)°	90·0°
β	98·58 (1)	98·21 (2)
γ	90·76 (1)	90·0
U	2043·8 Å^3	514·1 Å^3
Z	8	2
D_m	1·48 g cm^{-3}	
D_x	1·477	1·468 g cm^{-3}

Structure determination

Weak 'uneven reflexions' in the low-temperature phase are absent above the transition temperature. The intensity distribution is very much like that of 'even reflexions' in the low-temperature phase. The unit-cell dimensions a and b are approximately one half of those of the low-temperature phase and c is nearly the same. These observations suggest that the structure above the transition temperature is closely related to that of the 'average structure' in the low-temperature phase. Thus a set of starting coordinates was readily obtained from those of the low-temperature phase. Several cycles of block-diagonal least-squares refinement for all the atoms with isotropic temperature factors reduced R to 0·078. Further cycles of full-matrix least-squares refinement were carried out with anisotropic temperature factors for non-hydrogen atoms and isotropic

Table 2. *Atomic parameters of non-hydrogen atoms* ($\times 10^4$)

The values of β_{ij} refer to the expression $\exp[-(\beta_{11}h^2+\beta_{22}k^2+\beta_{33}l^2+2\beta_{12}hk+2\beta_{13}hl+2\beta_{23}kl)]$. Here and elsewhere in this paper the estimated standard deviations in the last figure are given in parentheses.

	x	y	z	β_{11}	β_{22}	β_{33}	β_{12}	β_{13}	β_{23}
Na	5000	5000	0	926 (14)	48 (1)	46 (1)	−14 (6)	111 (5)	2 (2)
C(1)	52 (6)	885 (2)	767 (2)	637 (22)	42 (2)	44 (2)	−45 (10)	13 (9)	16 (3)
C(2)	552 (7)	1099 (2)	−323 (2)	831 (25)	39 (2)	49 (2)	−44 (11)	35 (10)	19 (3)
C(3)	−496 (7)	−256 (2)	1056 (2)	850 (25)	45 (2)	40 (2)	−38 (11)	52 (10)	23 (3)
C(4)	102 (7)	1766 (2)	1532 (2)	790 (25)	39 (2)	42 (2)	−37 (10)	12 (10)	13 (3)
C(5)	−230 (7)	1545 (2)	2632 (2)	768 (25)	39 (2)	55 (2)	−19 (10)	20 (10)	4 (3)
C(6)	412 (7)	2909 (2)	1229 (2)	694 (24)	56 (2)	38 (2)	−15 (11)	34 (10)	1 (3)
N(1)	−462 (7)	1334 (2)	3517 (2)	1269 (27)	65 (2)	53 (2)	−2 (11)	110 (11)	2 (3)
N(2)	610 (6)	3827 (2)	950 (2)	1108 (25)	43 (2)	60 (2)	−12 (10)	108 (10)	15 (3)

Table 2 (*cont.*)

Atomic parameters of hydrogen atoms ($\times 10^3$)

	x	y	z	B (Å^2)*
H(1)	85 (7)	189 (2)	−54 (2)	4·7 (6)
H(2)	−87 (6)	−42 (2)	181 (2)	3·6 (5)

* Isotropic temperature factor.

ones for hydrogen atoms. The final R value became 0·033 for 675 reflexions. Unit weight was given to all the reflexions. The atomic scattering factors for non-hydrogen atoms were taken from *International Tables for X-ray Crystallography* (1962). The scattering factor curve of Stewart, Davidson & Simpson (1965) was used for hydrogen atoms. The final atomic parameters and their estimated standard deviations are listed in Table 2.*

Description of the structure and discussion

Fig 1(*a*) and (*b*) show projections of the structures of two modifications viewed along the *a* axis. Both structures are composed of columns of $TCNQ^-$ radical ions packed face-to-face along the *a* axis and sodium

* A table of structure factors has been deposited with the British Library Lending Division as Supplementary Publication No. SUP 30957 (6 pp.). Copies may be obtained through The Executive Secretary, International Union of Crystallography, 13 White Friars, Chester CH1 1NZ, England.

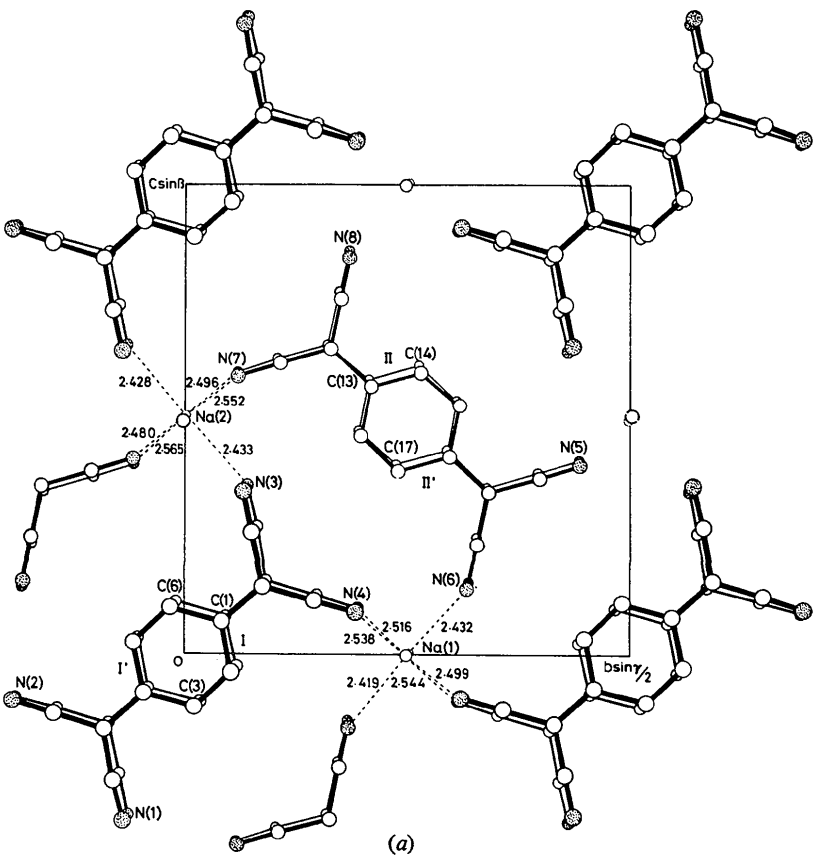

(*a*)

Fig. 1. Projections of the structures viewed along the *a* axis. (*a*) Low-temperature phase.

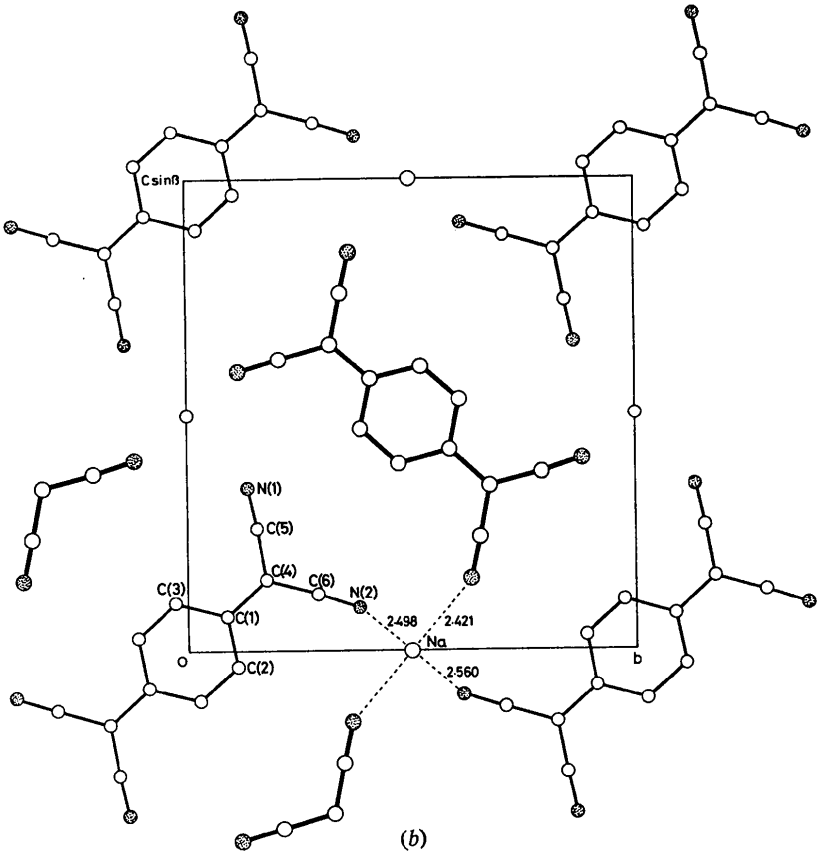

(*b*)

Fig. 1 (*cont.*) (*b*) High-temperature phase.

ions are arranged among the columns. A marked difference is observed in the structures of the TCNQ columns. In the high-temperature modification, the $TCNQ^-$ radical ions are packed with an equal interplanar distance of 3·385 Å; namely no dimeric $TCNQ^-$ units exist in the structure. In the low-temperature modification, however, there are two crystallographically independent columns, TCNQ (I) and TCNQ (II), in which $TCNQ^-$ radical ions are arranged with alternating interplanar distances as follows: TCNQ (I) 3·223, 3·505 Å; TCNQ (II) 3·200, 3·480 Å. Accordingly $TCNQ^-$ dimers occur in the structure with an interplanar spacing of 3·212 Å on the average. This may be the first example of monomer–dimer transition in a $TCNQ^-$ radical salt confirmed by means of X-rays. A $TCNQ^-$ radical is inclined at an angle of 74·5° with respect to the *a* axis above the transition temperature. This angle of inclination is nearly the same as those observed in the low-temperature modification.

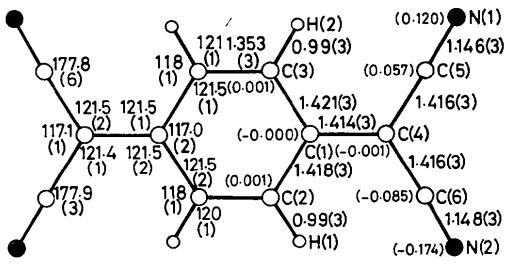

Fig. 2. Bond distances (Å) and bond angles (°) in the $TCNQ^-$ residue with their standard deviations. The numbers in parentheses are the atomic displacements from the mean plane through the quinodimethane moiety.

The molecular geometry is presented in Fig. 2. It possesses D_{2h} symmetry within the experimental errors and shows no significant differences as compared with that in the low-temperature modification. The shape and the size are consistent with those reported for $TCNQ^-$.

Fig. 3 illustrates the overlapping mode of adjacent TCNQ units. It is modified ring–ring overlap with a diagonal shift of the molecular centre. The same overlapping mode was observed between the dimeric units in the low-temperature phase. However, in the dimeric unit there was a modified ring–ring overlap with a shift of the molecular centre along its short axis.

The short contacts within a column are listed in Table 3. Fig. 4 gives an *ORTEP* plot of the thermal motion ellipsoids for TCNQ. The molecule exhibits the smallest thermal motion along the short axis. From Fig. 1 it can be easily seen that such a thermal motion is hindered by the sodium ions.

Table 3. *Relevant intermolecular distances* (Å)

The C···C and C···N distances less than 3·5 Å are listed. Key to symmetry operation: (i) $1+x, y, z$; between two adjacent TCNQ's.

C(2)···C(1^{i})	3·428 (3)	C(4)···C(5^{i})	3·485 (3)
C(5)···N(1^{i})	3·459 (3)		

A sodium ion is surrounded nearly octahedrally by the six negatively charged nitrogen atoms of different TCNQ ions. The Na...N distances are in the range 2·421 to 2·560 Å. The coordination geometry is very much like that of the low-temperature phase.

Passing through the transition temperature results in a remarkable change in the TCNQ columns: the dimeric structure transforms into a monomeric one. However, the arrangement of the sodium ions remains almost unchanged. The interplanar distance in the dimeric unit increases from 3·212 to 3·385 Å and the distance between the dimeric units decreases from 3·429 to 3·385 Å, resulting in a net elongation of the column. This is indicated by the change in cell dimensions. The length $2a$ of the high-temperature modification is about 0·4% greater than a of the low-temperature modification. The change means that the $TCNQ^-$ ions move along the column, accompanying a shift along the long axis of the molecule. Such molecular movements are in accord with the thermal motion ellipsoids of the TCNQ's which clearly show larger motion perpendicular to the molecular plane and along the long axis of the molecule.

In crystals of dark-purple Rb^+TCNQ^- (Shirotani & Kobayashi, 1973), $TCNQ^-$ ions are stacked face-to-face with an equal interplanar spacing of 3·42 Å but the overlapping mode is of the ring–external bond type which differs from the modified ring–ring overlap with the diagonal shift of the molecular centre found in the high-temperature modification of Na^+TCNQ^-. The

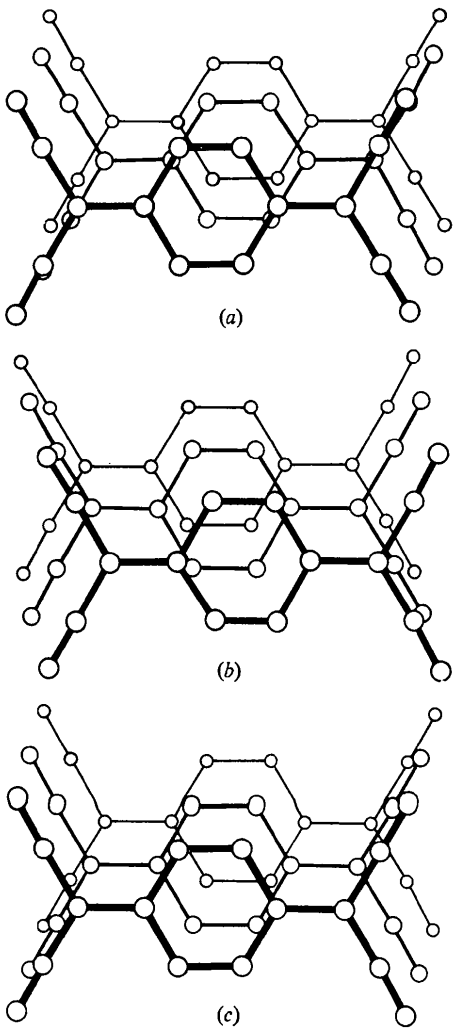

Fig. 3. The overlapping mode of adjacent TCNQ units. (*a*) Within a column of TCNQ I in the low-temperature phase. (*b*) Within a column of TCNQ II in the low-temperature phase. (*c*) Within a column of TCNQ in the high-temperature phase.

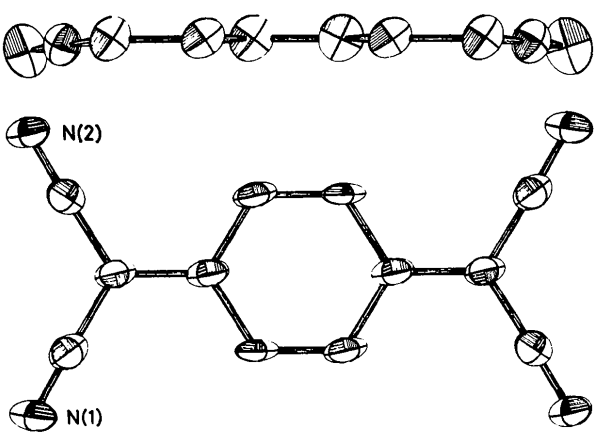

Fig. 4. The *ORTEP* plot of the thermal ellipsoids with probability of 50%.

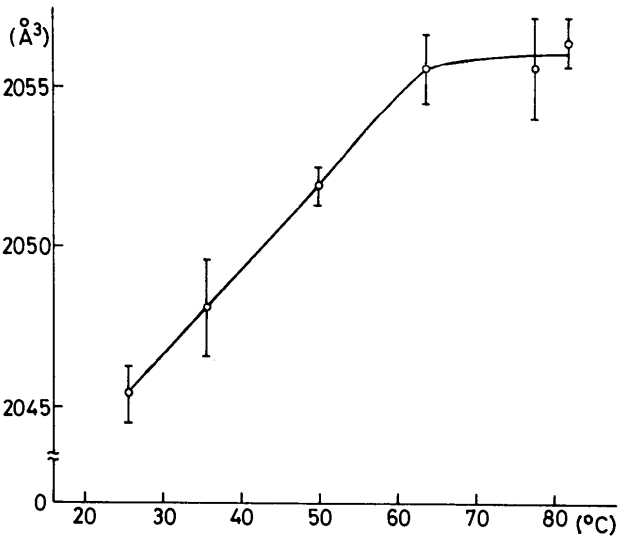

Fig. 5. The temperature variation of the unit-cell volume.

electrical conductivity of Rb^+TCNQ^- is much higher than that of Na^+TCNQ^- (Sakai, Shirotani & Minomura, 1972). This suggests that the overlapping mode of the $TCNQ^-$ ions may play an important role in the electrical conductivity.

Structural change with the transition

Fig. 5 represents the temperature variation of the unit-cell volume measured by means of a manual four-circle diffractometer, where four times that of the high-temperature phase is plotted for convenience. As the temperature rises, the volume increases continuously and no gap occurs at the transition temperature. In fact, the cell volume of the low-temperature phase becomes practically equal to four times that of the high-temperature phase at 62 °C. The ratios of the intensities of reflexions from the low-temperature phase to those at 26 °C are shown in Fig. 6. The ratio of the 200 reflexion of the high-temperature phase to that at 82 °C is also included in the figure. For these measurements, the crystal specimen was heated in an electric furnace and the temperature was controlled within ±0·3 °C throughout the experiment. Two neighbouring reflexions from the two individuals that form a rotational twin around the b^* axis are mostly well separated in the neighbourhood of the a^* axis in the reciprocal space. Accordingly, the intensities of an 'even reflexion',† 400, and a strong 'uneven reflexion',† $3\bar{1}0$, were selected for the measurement. In this case 400 and $\bar{4}00$ do not overlap. As the temperature is raised, the 200 reflexion of the high-temperature modification appears in the middle of 400 and $\bar{4}00$ at about 59 °C. With a further rise of temperature, the intensities of the reflexions from the low-temperature phase decrease rapidly, while that of 200 of the high-temperature phase increases. Above *ca* 73 °C, all the reflexions of the low-temperature phase vanish completely and only 200 of the high-temperature phase remains. The observed changes in intensities of these reflexions were completely reversible and no hysteresis was observed. From these observations it may be said that the phase change is essentially first order.

† See Konno & Saito (1974).

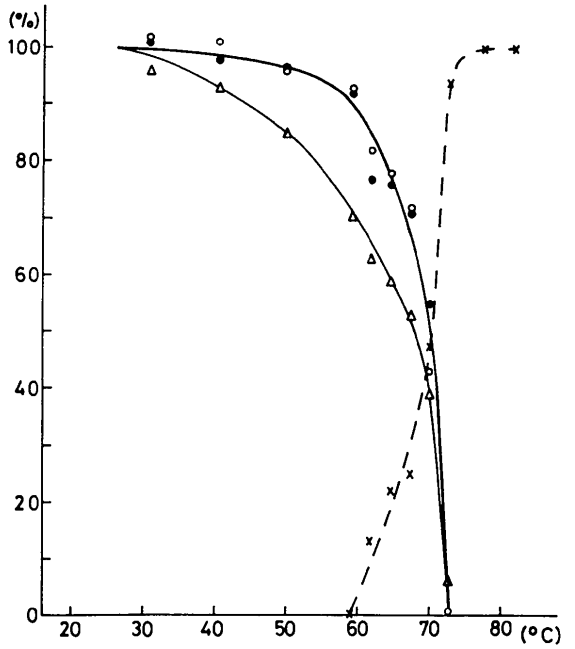

Fig. 6. The temperature dependence of the intensity ratios, $I(hkl)_{t°}/I(hkl)_{26°}$ of the low-temperature phase and that of $I(200)_{t°}/I(200)_{82°}$ of the high-temperature phase. ○: 400, ●: $\bar{4}00$, △: $3\bar{1}0$, ×: 200.

The observed temperature variations indicate that the high-temperature phase appears at about 59 °C and grows with a rise of temperature at the cost of the low-temperature phase and finally above 73 °C only the high-temperature phase remains. Thus both phases coexist in the temperature range from 59° to 73 °C.

It can be easily shown that the intensity of 'uneven reflexions' depends upon $(\mathbf{H} \cdot \Delta\mathbf{r})$, where $\mathbf{H}$ stands for a reciprocal vector and $\Delta\mathbf{r}$ represents the displacement of the molecular centre of $TCNQ^-$ from 'average structure', which is monomeric. In particular, the intensity of $3\bar{1}0$ is mostly due to the contribution of $TCNQ^-$ radical ions and the contribution of Na^+ is small. As shown in Fig. 6, $3\bar{1}0$ begins to decrease at about 30 °C. $3\bar{1}0$ and 400 decrease very rapidly to zero above 59 °C, where the high-temperature phase begins to appear. This indicates that some structural change may have already occurred in the TCNQ columns around 30 °C. However, a rigorous monomeric structure will not be realized until the high-temperature phase appears above 59 °C. As shown in Fig. 6, the low- and high-temperature phases coexist in the range 59 to 73 °C. The energy loss arising at the boundary surface between the two phases may be quite small and the energy gain due to mixing entropy would compensate for it, giving rise to the coexistence of the two phases. This phenomenon might correspond to the model proposed by Frenkel (1947) and Sorai & Seki (1974). The twinning observed in the low-temperature modification is suggestive of a small energy loss.

All the computations were performed on the FACOM 270–30 at this Institute with a local version of the Universal Crystallographic Computation Program System, UNICS, 1967, Crystallographic Society of Japan. Part of the cost of this research was met by a Scientific Research Grant from the Ministry of Education, to which the authors' thanks are due.

References

FRENKEL, J. (1947). *Kinetic Theory of Liquids*, Chap. 7, London: Oxford Univ. Press.

International Tables for X-ray Crystallography (1962). Vol. III, 2nd ed. Birmingham: Kynoch Press.
KONNO, M. & SAITO, Y. (1974). *Acta Cryst.* B30, 1294–1299.
SAKAI, N., SHIROTANI, I. & MINOMURA, S. (1972). *Bull. Chem. Soc. Japan*, **45**, 3314–3320.
SHIROTANI, I. & KOBAYASHI, H. (1973). *Bull. Chem. Soc. Japan*, **46**, 2595–2596.
SORAI, M. & SEKI, S. (1974). *J. Phys. Chem. Solids*, **35**, 555–570.
STEWART, R. F., DAVIDSON, E. R. & SIMPSON, W. T. (1965). *J. Chem. Phys.* **42**, 3175–3187.
VEGTER, J. G., KUINDERSMA, P. I. & KOMMANDEUR, J. (1971). *Conduction in Low-Mobility Materials*, edited by N. KLEIN, D. S. TANNHAUSER & M. POLLAK, pp. 363–373. London: Taylor and Francis.

Acta Cryst. (1975). B31, 2012

The Crystal Structure of Hexagonal $BaSrFe_4O_8$

BY M. C. CADÉE

Gorlaeus Laboratories, Section of Solid State Chemistry, University of Leiden, P.O.Box 75, Leiden, The Netherlands

(*Received* 23 *October* 1974; *accepted* 24 *February* 1975)

The structure of hexagonal $BaSrFe_4O_8$ was redetermined and found to be isostructural with $BaCaFe_4O_8$ (space group $P\bar{3}1m$). Mössbauer spectra and magnetic measurements showed $BaCaFe_4O_8$ and $BaSrFe_4O_8$ to be anti-ferromagnetic, with a Neël temperature higher than 1000K. Ca^{2+} can be substituted by Sr^{2+} only, Fe^{3+} partially by Al^{3+} and Ga^{3+}.

Introduction

Hexagonal $BaSrFe_4O_8$ was first reported by Kanamaru & Kiriyama (1964). In a determination of the crystal structure (Lucchini, Minichelli & Meriani, 1973) a structure related to that of $BaAl_2O_4$ (Wallmark & Westgren, 1937) was found. The X-ray powder diffraction patterns of hexagonal $BaSrFe_4O_8$ prepared by us showed that this compound could be isostructural with $BaCaFe_4O_8$ (Herrmann & Bacmann, 1971). Comparison of the unit-cell dimensions supported this conclusion. Relating the structure of $BaSrFe_4O_8$ to the structure of $BaAl_2O_4$, the c axis is expected to be about 8·6 Å [mean value of the c axis of $BaAl_2O_4$ and $SrAl_2O_4$ (Glasser & Dent-Glasser, 1963)]. The unit-cell dimensions of these compounds are presented in Table 1.

Table 1. *Unit-cell dimensions* (Å) *of some hexagonal* AB_2O_4 *compounds*

Compound	a	c	Reference
$BaAl_2O_4$	5·209	8·761	Wallmark & Westgren (1937)
$SrAl_2O_4$	5·10	8·49	Glasser & Dent-Glasser (1963)
$BaCaFe_4O_8$	5·407	7·703	Herrmann & Bacmann (1971)
$BaSrFe_4O_8$	5·448	8·091	Lucchini, Minichelli & Meriani (1973)
$BaSrFe_4O_8$	5·446	8·082	This publication
$BaSrFe_4O_8$	5·15	8·62	Expected for $BaSrFe_4O_8$ related to $BaAl_2O_4$

Experimental

Commercially available $BaCO_3$, $SrCO_3$ and Fe_2O_3 (P. A.) were thoroughly mixed in an agate mortar under acetone and then fired at 1000 °C for one day, reground and fired twice for several days and finally fired at 1000 °C for two weeks. The X-ray powder diffraction pattern showed one phase and could be indexed as hexagonal with unit-cell dimensions $a=5{\cdot}4464(9)$ and $c=8{\cdot}0817(14)$ Å (the numbers in parentheses giving the standard deviation in units of the last decimal). No systematic absences were found. X-ray intensities were collected from a powder pattern of all reflexions between 5 and 110° in 2θ, recorded with a Philips diffractometer, using Cu $K\alpha$ radiation with a graphite monochromator.

Models

Five starting models of the $BaSrFe_4O_8$ structure were chosen for a least-squares refinement. The ion positions are shown in Fig. 1 and Table 2.

Model 1 (Fig. 1*a*) is isostructural with $BaCaFe_4O_8$, spacegroup $P\bar{3}1m$ with the layer sequence BaO_2, O_3, $Sr\diamond\diamond$,* O_3 and BaO_2. The layers are h.c.-stacked. The Fe^{3+} ions are between the BaO_2 and the O_3 layers, in a tetrahedron of O^{2-} ions. The Sr^{2+} ion is surrounded by six O^{2-} ions, forming an octahedron. The Ba^{2+} ion is surrounded by 12 O^{2-} ions.

* The symbol $\diamond$ means an oxygen vacancy.